

Microfabrication by localized electrochemical deposition: experimental investigation and theoretical modelling

R A Said

Electrical Engineering Department, United Arab Emirates University, PO Box 17555, Al-Ain, Abo-Dhabi, United Arab Emirates

E-mail: rasaid@uaeu.ac.ae

Received 27 November 2002, in final form 24 February 2003

Published 31 March 2003

Online at stacks.iop.org/Nano/14/523

Abstract

Adding to the efforts spent to establish localized electrochemical deposition (LECD) as a standard fabrication process; this paper presents an experimental investigation and theoretical modelling of shape formation of high aspect ratio columns and lines fabricated by LECD. The proposed model suggests that transport of depositing ions leading to deposit formation is mainly dominated by migration forces. The deposition model is verified by numerical simulation which utilizes electric field calculation by a boundary element method and a progressive boundary update approach to determine the evolution of deposition profiles. Simulation results are compared against images of copper columns obtained at different formation stages during the deposition process. Both results are in agreement, which demonstrates the potential and capabilities of the proposed model and simulation procedures as an analysis tool to aid in characterizing the deposition process and resulting structures, as well as the understanding of the dynamics and factors influencing object formation in LECD.

(Some figures in this article are in colour only in the electronic version)

1. Introduction

The ability to fabricate microstructures with controlled and confined geometries is essential to meet technological demands in continuously reducing structural dimensions. Structures with high aspect ratio features are of particular importance since they enable a wide range of applications in microelectronics and instrumentation [1], communications [2–4], microrobotics [5], life science [6, 7], integrated hydrodynamic and thermodynamic microsystems [8, 9] and countless applications utilizing microsensors, actuators and miniature devices.

Of interest to this work are three-dimensional (3D) high aspect ratio objects with geometries such as lines and columns of arbitrary trajectories, helices, tubes etc. Although such structures attract interest for a broad range of applications and research in different fields, they are of particular interest in the present work for the realization of electrically conducting objects for rapid prototyping and fixation of integrated circuits (ICs), ICs interconnects and

rerouting [10] and antenna elements for integrated transceiver communication systems [11].

Realization of the above-mentioned objects at the micrometre and sub-micrometre scale is still a considerable challenge. Current fabrication techniques capable of producing high aspect ratio structures can generally be grouped as batch patterning techniques and probe directed techniques. Batch patterning techniques rely on the use of a mask or a mould to confine and shape batches of deposited or removed material. Lithography [12] and electrodeposition [13], among other techniques mainly driven from the silicon-based electronics industry, are examples of processes that require the use of a mask to build rather two-dimensional (2D) planar structures. High aspect ratio geometries are thus a result of multiple steps of material deposition or removal through the use of several masks, which adds to the required fabrication time and cost.

Probe directed techniques, many of which are still under development, overcome some of the above limitations.

Unlike batch patterning techniques, probe directed methods utilize a miniaturized probe to initiate and enhance material growth from a surrounding medium directly at the end of the probe. Moving the end of the probe relative to a reference point allows the production of arbitrary geometries. Examples of probe techniques include laser assisted chemical vapour deposition (LACVD) [14], where a laser beam is used as the probe to provoke material deposition from a surrounding vapour. The resolution achieved by LACVD is limited by the diffraction of the laser beam used. A similar technique that induces microfabrication uses an electron beam as a probe [15]. Recently a localized electrochemical deposition (LECD) technique [16] has been introduced in which a conducting microelectrode is used to fabricate high aspect ratio structures.

LECD has many of the technical and economical advantages associated with electrodeposition (electroplating) technology [17]. Specifically, LECD is applicable to many materials without limitations on the type or size of the substrate or the type or thickness of deposited material [18]. LECD, however, is capable of providing deposition rates of the order of several $\mu\text{m s}^{-1}$ and can reach more than $30 \mu\text{m s}^{-1}$ with the aid of a jet mechanism [19].

During fabrication, localized deposition is produced by placing an electrode tip, which has micrometre-scale dimensions, near a substrate in an electrolyte and applying an electric potential between them [20]. Due to the highly localized electric field in the region between the microelectrode and the substrate, confined deposition is produced. High aspect ratio structures result from the displacement of the end of the electrode along the trajectory of the desired geometry while maintaining continuity with the deposited material.

Efforts invested in developing LECD as a standard fabrication technique have concentrated on demonstrating its capabilities [10, 20–22]. The technique has been demonstrated on conducting, semiconducting, and non-conducting substrates [23]. Geometries of microstructures fabricated by LECD have been achieved using a glass-insulated ultra-microelectrode (UME) tip [19], the tip of an atomic force microscope (AFM) [20, 24] and a micropipette electrode [25], thus allowing fabrication at micrometre and sub-micrometre scales. Investigation of the effect of different parameters of the LECD process on the deposition rate and characteristics of deposited structures has also been presented. Among the investigated parameters are the applied electrode potential, electrolyte concentration, the presence of organic additives [26], rotating the electrode tip [27], the presence of ultrasonic vibrations during deposition [28] and the effect of insulation material surrounding the electrode tip [29]. Study of these effects has been mainly experimental in nature but without quantitative modelling.

Attempts to model the localized deposition process have generally been limited to the estimation of the electric field distribution on the substrate due to a nearby microelectrode [20]. A quantitative evaluation of the progressive formation of the localized deposit is necessary for the characterization of the LECD process and the resulting structures. Such calculations will also provide a better understanding of the deposition dynamics to further enhance many of the LECD characteristics such as the process rate and

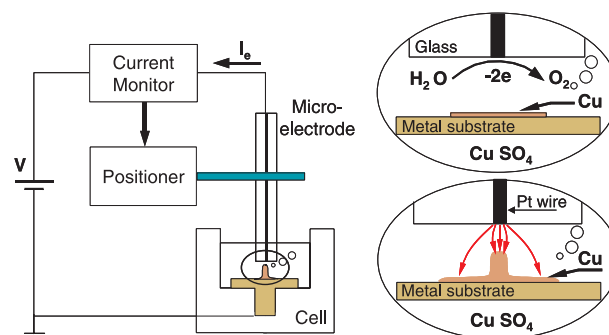


Figure 1. An illustration of a typical LECD set-up arrangement, including reaction-current monitoring for feedback and probe positioning purposes. The concept of localized deposition is illustrated by circled drawings demonstrating an oxidation reaction at the microelectrode end (anode), thus causing bubbles, and a reduction reaction at the substrate (cathode) resulting in copper deposition. An intense electric field causes faster deposition rates beneath the microelectrode end, hence localizing the deposition.

repeatability, dimensional confinement, structure porosity and quality of results.

This work presents both experimental investigation and theoretical modelling of shape formation in microstructures fabricated by LECD. The most fundamental and simplest of these structures are lines and columns which are considered here. The proposed simulation procedures rely on determining incremental growth of the deposition from electric potential calculations using the boundary element method. The evolution of shape formation is enabled using a progressive boundary update approach. Simulation results are compared with images of the evolution of copper columns at different formation stages. The comparison of both results reveals the quality of the simulation results, indicating its promise for further studies of the characterization of the LECD process.

2. Localized electrochemical deposition

2.1. Principle of operation

The schematic drawing in figure 1 illustrates a general arrangement of a typical set-up used for LECD. A microelectrode is placed very close to a conducting substrate, while both are immersed in an ionically conducting electrolyte that contains ions of the material to be deposited. The microelectrode is usually insulated from all sides except for an exposed tip region with micrometre-scale dimensions. An electric potential is applied between the microelectrode and the substrate, thus causing a faradic current to flow through the electrolyte between the microelectrode and the substrate. Since the electrolyte contains reducible metal ions (e.g. Cu^{2+} ions in the present work) and the substrate is connected to a negative potential with respect to the microelectrode, then the flow of faradic current results in an oxidation process at the microelectrode tip and a deposition of metal ions at the substrate, as illustrated by the circled drawings in figure 1.

Unlike typical electroplating methods, where deposition occurs at a uniform rate on all exposed regions of the substrate, the deposition process outlined in figure 1 is very localized to the region beneath the electrode tip. This is due to the highly

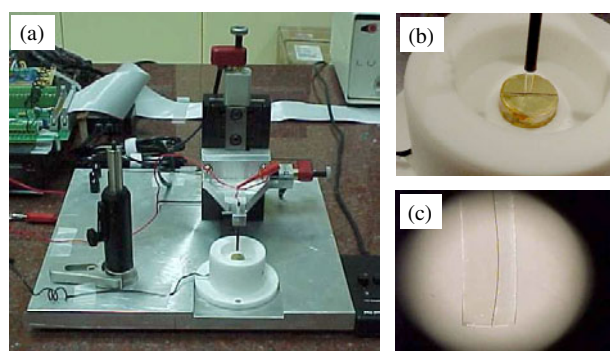


Figure 2. Photographs of (a) the constructed LECD apparatus showing the aluminium base, the Teflon cell and the three-axis positioning stage holding the microelectrode, (b) a close-up of cell-substrate-probe arrangement and (c) an optical microscope photograph of the glass insulated microelectrode showing the 25 μm diameter Pt wire.

localized electric field in the space between the microelectrode tip and the substrate region directly below the tip. The result is highly localized growth with an extent of approximately the dimensions of the microelectrode tip, as illustrated by the lower circled drawing in figure 1. At the start of fabrication, however, the extent of deposition is usually less confined and extends outside the region beneath the tip due to a fringing electric field emanating from the tip boundaries and terminating on the substrate, which will be demonstrated in the next section. As the deposition end moves farther away from the substrate, the geometry of the deposit becomes more confined to a region of the same extent as the tip boundaries.

The deposition rate in the LECD process is proportional to the magnitude of the deposition current which is monitored during the entire fabrication session. The magnitude of the deposition current can be controlled by adjusting the space between the microelectrode tip and the substrate using conventional feedback control along with a positioning mechanism for electrode displacement. During deposition, the microelectrode is moved with respect to the deposition end along the trajectory of the desired microstructure geometries.

2.2. Instrumentation and demonstration

The photographs in figure 2 show the details of a constructed apparatus used for LECD fabrication. The apparatus consists of an aluminium base holding a deposition cell, machined from Teflon, and the microelectrode mounted on a three-axis positioning stage. The microelectrode used in the present work was prepared from a 25 μm in diameter Pt wire following the procedures outlined in the literature [30]. The Pt wire was inserted in a glass micropipette that was sealed to insulate the wire from all sides except at the very end of the wire, which was polished to form an exposed disc. Electrode polishing was done using successive grades of 600, 1200 and 1500 silicon carbide paper and final polishing with 1.0 μm diamond polish followed by 0.05 μm alumina to produce a smooth surface with nanometre-scale roughness. The glass surrounding the electrode wire extends to a diameter of about 1500 μm . The three-axis positioning stage uses microstepping motors (New Focus, Inc., CA, USA) capable of very fine steps, around

30 nm, achievable at various speeds with a maximum of 28 $\mu\text{m s}^{-1}$.

As a demonstration, the deposition of copper columns and lines was attempted on metal substrates using the apparatus in figure 2 and an electrolyte of copper sulfate solution ($\text{CuSO}_4 \cdot 5\text{H}_2\text{O}$, 250 g l^{-1}). The substrates were prepared from 1.0 cm diameter metal rods that were cut and machined as a T-section that fits and locks into the Teflon cell. The substrate surfaces were polished with successive grades of 240, 400 and 600 silicon carbide paper. Final polishing was done using diamond polishing paste and then alumina, as in the electrode preparation.

Upon fabrication, the deposition cell was filled with the electrolyte and the electrode tip brought close to the substrate surface. An electric potential was applied to the tip with the substrate grounded and a feedback circuit used to move the tip away from the growing copper as it touches the tip. The feedback circuit operates by setting a reference potential V_0 (equivalent to a reference deposition current I_0) and comparing it with the monitored deposition current. As deposition is started, copper grows on the substrate beneath the tip, causing the deposition current through the tip I_t to increase until the growing copper touches the tip at which I_t exceeds I_0 . This triggers the feedback circuit to move the tip away from the deposition end and along the desired trajectory at a constant speed until the reference current value I_0 is restored, at which tip displacement is stopped. Copper growth continues until the growing metal touches the tip again, which triggers the feedback circuit to move the tip, and so on. Figure 3 shows scanning electron microscope (SEM) images of examples of a fabricated copper column and line deposited under an applied potential of 4.0 V. The objects in figure 3 have a diameter of about 25 μm and lengths ranging from few hundred micrometres to few millimetres.

Due to the high aspect ratio of their geometries, the ability of column structures such as those shown in figure 3 to withstand impact forces, during sample handling for example, becomes a concern. A major factor affecting this is the adhesion of deposited structures to the substrate. In an attempt to evaluate the adhesion force holding a deposited column to the substrate, the average force, applied at the top end of the column, required to release the column from the substrate, was measured. In the force measurement the electrode structure and one of the positioning stage axes were arranged and used to apply a force at the top end of the column, perpendicular to its axis and parallel to the substrate. Here, the electrode end was pushed against the column end by triggering the positioning axis to move incremental steps of 30 nm continuously until the column is released from the substrate. This was repeated for several columns of heights around 500 μm . On average, the columns were released from the substrate after the positioning axis (and correspondingly the column end) had moved about 0.5 μm . The force exerted at the column end can be extracted using the displacement of the column end and the spring constant k of the column, which can be evaluated using [31] $k = (3\pi E a^4)/4l^3$, where E is the modulus of elasticity of the column material ($E = 110$ GPa for copper), a is the column's radius and l its length. Using a column radius of 12.5 μm and length of 500 μm , the force exerted at the column end to release it from the substrate is evaluated as 25.3 μN . This is

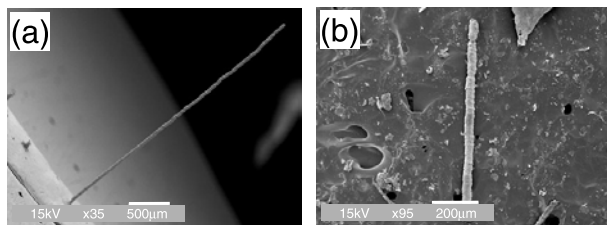


Figure 3. SEM images of high aspect ratio copper column ($\varnothing = 25 \mu\text{m}$, length $> 2 \text{ mm}$) (a) and a copper line (b) fabricated using the apparatus in figure 2 and copper sulfate solution.

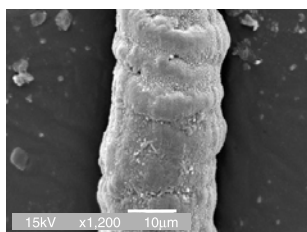


Figure 4. SEM image of a section of the line presented earlier in figure 3, showing pulsed-like deposition, suggesting consistent electrode displacement of $5 \mu\text{m}$.

equivalent to attaching $2600 \mu\text{g}$ at the end of the column while protruding horizontally out of a vertical substrate.

2.3. Experimental observations

Several properties and observations on fabrications produced by LECD have been presented in earlier experimental studies [20, 26–28]. This work focuses on two observations related to the shape formation of deposited structures. The first is the pulsed-like structure that can be noted in the SEM images in figure 3 and the enlarged image shown in figure 4. This is explained by the adopted feedback mechanism described earlier. The image suggests pulsed deposition intervals of $5 \mu\text{m}$, which corresponds to the value of the set reference current I_0 that determined the initial separation between the tip and substrate.

The other observation of importance to this work is the large dimension of the base of fabricated columns in figure 3 as compared with the column or tip diameters. To illustrate this, figure 5 shows SEM images of $25 \mu\text{m}$ diameter columns of about $150 \mu\text{m}$ length, and enlarged images of the corresponding column bases. As is obvious from the images in figure 5, appreciable deposition at the start of fabrication (column base) extends way beyond the desired region (within a tip diameter). As column formation proceeds and deposition grows, however, evolved geometry becomes more confined to the desired dimensions. The undesirable deposition growth shown in figure 5 would limit the resolution of the LECD process, especially when considering array structures. Moreover, this may affect the structure's performance in geometry-dependent applications, and can lead to malfunction of integrated structures due to electric shorts between adjacent objects used in electrostatic or high-frequency applications.

The undesirable deposition shown in figure 5 can be explained by the concentrated fringing field lines around the tip for a small tip–substrate spacing at the start of

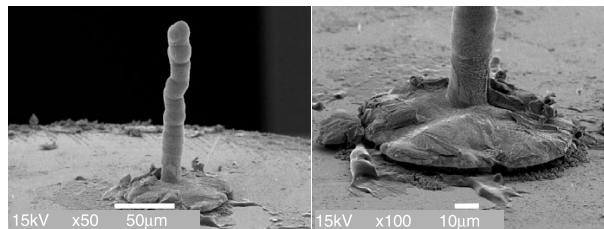


Figure 5. SEM images of deposited copper microcolumns, illustrating the large dimensions of the columns bases, which may limit the resolution of the fabrication by LECD.

fabrication. The density of fringing field lines, however, decreases as the deposition grows and the tip achieves a large separation from the substrate, hence localizing deposition (increasing deposition rate) to the region directly beneath the tip. The descriptive nature of this explanation, however, is not sufficient to provide a quantitative analysis of shape formation during deposition. Moreover, a quantitative analysis is required to aid in finding methods for controlling deposit formation.

3. Shape formation

3.1. Experimental investigation

In order to model deposit formation in LECD, column formation was first investigated experimentally. In the experiments a series of column depositions were attempted following the procedures outlined in the previous section. The deposition of each column in the series, however, was stopped one tip-displacement step farther than it was stopped at the deposition of the preceding column case. Elapsed deposition time was not considered in determining deposition height, since deposition rate varies in any deposition session due to vigorous bubble formation at the microelectrode tip during deposition that tends to insulate the tip from the electrolyte and prevents deposition current and material reduction from occurring. Figure 6 shows SEM images of deposition results for three different stages of column formation corresponding to deposition heights of 5 , 15 and $30 \mu\text{m}$.

The images in figure 6 illustrate two rates of deposition, one in the region within a virtual cylindrical boundary that has a diameter almost equivalent to that of the tip, and another region that extends outside this boundary. The deposition profiles in all the side-view images in figure 6 demonstrate a steady deposition rate within the cylindrical boundary, which contributes to the desired column growth. The deposition rate outside this region tends to be highest for tip–substrate spacings much smaller than the tip diameter, as in figure 6(a) ($5 \mu\text{m} \ll 25 \mu\text{m}$), and decreases as the tip is displaced farther away from the substrate. This is clearly evident from the wide spread of deposition around the column base in figure 6(a), which evolves into the volcano shape in figure 6(b) that indicates a substantial decrease in the rate of side deposition at such a tip–substrate spacing ($15 \mu\text{m}$), and becomes extremely slow for tip–substrate spacings of the same order as or larger than the tip diameter ($30 \mu\text{m} > 25 \mu\text{m}$) as in figure 6(c). At this column height and afterwards the deposition rate is much faster directly beneath the tip, with depositions outside

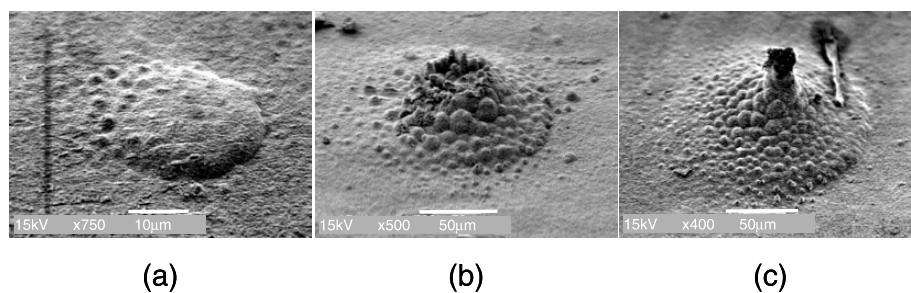


Figure 6. SEM images showing the evolution of a copper column at different stages of formation. The shown depositions were formed separately with the deposition stopped when the deposited column height reached (a) 5 μm , (b) 15 μm and (c) 30 μm , without consideration of the required deposition time.

the intended boundaries still occurring but at a much slower rate (determined by the steady-state limiting current of the tip at infinite tip–substrate spacing [30]).

3.2. Deposition profile modelling

In order to study the effect of the different possible factors enabling the undesirable side deposition in figures 5 and 6, it is necessary to quantitatively determine deposition profiles resulting during LECD microfabrication. This section proposes a model for shape formation in LECD and simulation procedures to determine the corresponding incremental growth.

Quantitative determination of shape formation in locally deposited structures can be treated by calculating deposition current distribution typically encountered in problems involving change in electrode shape, such as in electroforming, electrochemical machining and other electrochemical processes [33–38]. In such problems, the anode (equivalent to the microelectrode in this work) is stationary and the changing boundary is only that of the cathode (the substrate) due to a deposition or etching process. In the simulation of localized deposition considered here, however, the microelectrode is repeatedly displaced away from the deposition surface as deposition growth reaches the microelectrode tip. Thus, the boundaries of both the cathode and the anode in LECD are continuously changing due to incremental deposition on the substrate and the displacement of the microelectrode relative to the deposition end.

The deposition of ions from an electrolyte is usually controlled by four partial reactions [39] including: mass transport, charge transfer, chemical reaction and crystallization. Understanding of these partial reactions and their effect on the deposition rate is well established in the literature [40]. Essentially, an ion must have enough energy to transport through the bulk electrolyte and reach the electrode/solution interface, overcome the potential barrier at the interface, receive an electron to neutralize as an atom, and incorporate itself within the crystal of other atoms reduced from the electrolyte. In this series of events, mass transport and charge transfer are generally the limiting factors of deposition rate [41]. Charge transfer is directly affected by the applied electrode potential, and for typical electric potentials used in LECD, charge transfer rates greatly exceed that of mass transport, thus leaving it as the rate-determining process.

The three mechanisms of mass transport are: convection (in both of its forms: natural and forced) that is driven by pressure gradient, diffusion by concentration gradient and migration by electric potential gradient. Unless enhanced by a jet mechanism, mechanical stirring, or heat-induced microstirring, convection-based mass transport plays a minor role in determining the deposition rate in LECD. Both diffusion and migration, on the other hand, greatly determine the rate of transfer of depositing ions from the bulk electrolyte to highly depleted regions between the electrode tip and the substrate. Since the electric field in this region is highly intense ($\approx 10^6 \text{ V m}^{-1}$ at 1 μm tip–substrate spacing), depositing ions will be mainly directed by migration forces; this has never been verified by a comparison between observed deposition profiles and calculated electric field strength for a disc electrode over a flat substrate [20]. Thus, the determination of shape formation and resulting deposition profiles can be achieved by adopting a simplified deposition model based on determining the electric field distribution in the region between the electrode tip and the substrate, assuming 100% deposition efficiency resulting from the force exerted by the electric field on depositing ions.

The deposition model suggested above applies to electrode–substrate arrangements where the tip–substrate spacing is much smaller than the tip diameter. This is necessary to ensure the domination of the migration mechanism in determining shape formation. Figure 7 shows an example of such an arrangement that also schematically illustrates the model considered for shape formation in column deposition. To complete the deposition model, and simplify the formulation of determining the shape formation, the following assumptions are considered:

- (1) a single depositing species is involved in the deposition reaction (copper ions in this work),
- (2) the bulk of the electrolyte is well stirred so that no concentration gradients are present,
- (3) the diffusivity of the reacting species is constant during the deposition and that the rate of change of shape of the deposit is slow compared with the establishment of the concentration field, and
- (4) deposition current efficiency is unity.

Quantitative determination of shape formation and the corresponding deposition profiles can be evaluated from the deposition surface velocity resulting from deposition growth. The local surface velocity (proportional to the deposition rate), v_s , at any coordinates of the depositing surface, in a direction

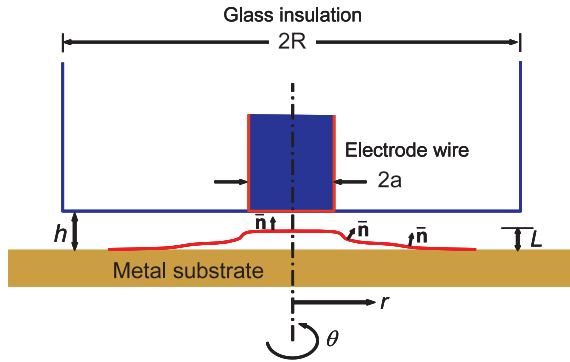


Figure 7. A schematic illustration of the microelectrode and substrate arrangement considered for modelling shape formation in column deposition. The model assumes an infinite substrate and tip–substrate spacing much smaller than the diameter of the electrode wire ($h \ll 2a$).

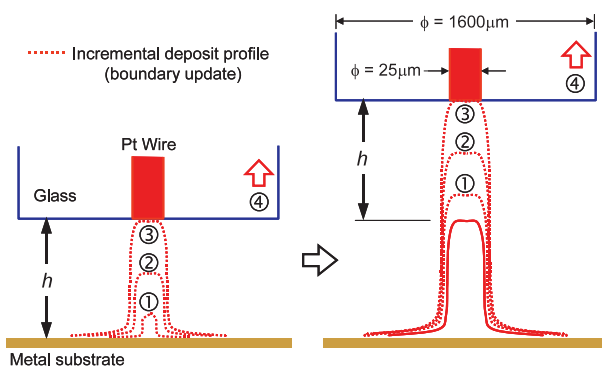


Figure 8. A drawing illustrating the sequence of calculation procedures followed in the proposed progressive boundary update approach. Incremental deposition profiles are evaluated from electric field calculation (using updated boundaries) while the electrode is held at a constant height ‘ h ’ above the substrate. The microelectrode is raised by another displacement ‘ h ’ when deposition height reaches the end of the electrode.

of the surface normal \vec{n} , indicated in figure 7, can be described by Faraday’s law as [40]

$$\vec{n} \cdot \mathbf{v}_s = \frac{M}{\rho z F} i_n, \quad (1)$$

where M is the atomic weight (g mol^{-1}) of depositing species, ρ is its density (g m^{-3}), z is the number of electrons in the deposition reaction, F is the Faraday number (96,500 C) and i_n is the deposition current density (A m^{-2}) normal to the surface. At the deposition boundaries the normal current density is proportional to the gradient of the electric potential, ϕ [40]

$$i_n = -\kappa \nabla_n \phi, \quad (2)$$

where κ is the electrolyte conductivity ($\Omega^{-1} \text{m}^{-1}$), and ∇_n is the gradient operator component normal to the deposition surface. Substituting for the deposition current in (1) from (2) gives

$$\vec{n} \cdot \mathbf{v}_s = -\frac{M\kappa}{\rho z F} \nabla_n \phi. \quad (3)$$

Using the identity $-\nabla_n \phi = E_n$, where E_n is the component of the electric field intensity (V m) normal to the deposition

surface, equation (3) can be rewritten as

$$\vec{n} \cdot \mathbf{v}_s = \frac{M\kappa}{\rho z F} E_n. \quad (4)$$

Thus, the deposition profile represented by the deposition surface velocity can be determined from the normal gradient of the electric potential as in equation (3), or equivalently from the electric field component normal to the deposit surface as in equation (4). The electric potential is governed by Laplace’s equation:

$$\nabla^2 \phi = 0, \quad (5)$$

which applies to the electric potential distribution in the electrolytic solution. The expression in equation (5) can be solved using available numerical techniques and using proper boundaries representing the microelectrode–substrate arrangement shown in figure 7. A review of the implementation of different numerical techniques in applications relevant to electrochemical deposition as well as a description of the advantages and limitations of each technique is documented in the literature [42]. In the presented work, a numerical computational code based on the boundary element method [43] is used to solve for the electric potential. The calculated potential distribution is then used to determine the electric field distribution and consequently the deposition profile according to (4).

3.3. Progressive boundary update method

The calculation procedures outlined in the deposition model proposed above are for stationary tip-deposition geometries. The evolution of the deposition growth, and consequently the deposition profile at different deposition thicknesses (column heights in this work), can only be obtained through updated calculations of deposition increments. The displacement of the electrode tip must also be coordinated in order to simulate the actual electrode positioning. This sequence of calculation procedures is referred to here as the progressive boundary update method, which is illustrated by the schematic drawing in figure 8. The steps followed in this method can be summarized by the following:

- (1) Initially, the microelectrode tip is placed at a distance h above the substrate and the calculation procedures outlined in the previous section are carried out to determine the profile of the first incremental deposition.
- (2) The maximum increment of the calculated deposition profile is chosen to be smaller than h . The determined profile is then considered as the new boundary of the substrate while the microelectrode is kept at the same distance h from the original substrate boundary.
- (3) The calculation procedures are carried out again to determine the profile of the new incremental deposition, which is then added to the previous profile to update the profile of the deposition.
- (4) These procedures are repeated to progressively update the deposition profile until a region on the deposition profile comes into contact with the microelectrode tip. At this stage, the microelectrode is displaced a distance h from the highest point on the latest profile.

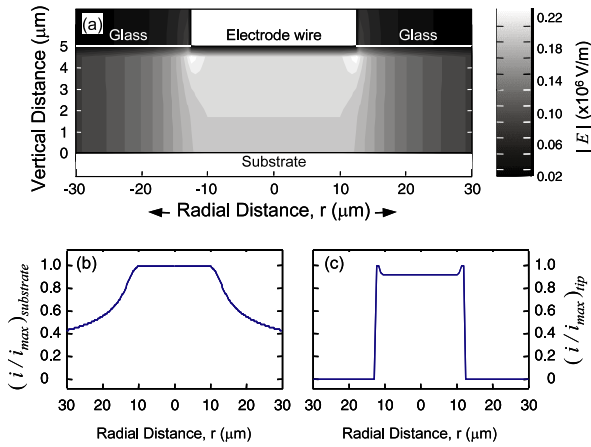


Figure 9. Quantitative evaluation: (a) electric field distribution in the space between a probe electrode, $2a = 25 \mu\text{m}$, and a flat substrate at a spacing of $5 \mu\text{m}$ between them; (b) and (c) the normalized deposition current densities at the substrate and tip surfaces respectively.

- (5) The calculation procedures are repeated in the same fashion described earlier to progressively update the deposition profile. This is continued until the deposition growth has reached the tip before any new displacement of the microelectrode.

4. Results and analysis

Using the deposition model and the calculation procedures proposed earlier, the distribution of the electric field intensity between a microelectrode ($2a = 25 \mu\text{m}$ and $2R = 1500 \mu\text{m}$) and an approximately infinite substrate was calculated with $5 \mu\text{m}$ space between them. Figure 9(a) shows the distribution of the electric field in a plane perpendicular to the substrate and the surface of the tip. The results in figure 9(a) demonstrate a highly intense and localized electric field at a tip-substrate spacing of $5 \mu\text{m}$ with the field dropping to half of its maximum (the maximum field is at the edge of the tip) at a radial distance of about $1.8 \times$ the tip diameter. The resulting current density both at the substrate and the tip surface is shown in figures 9(b) and (c) respectively. As expected, the maximum deposition current on the tip surface occurs at the edges.

To demonstrate the ability to determine shape formation in LECD, the deposition profile of a column structure over an infinite substrate was simulated using a probe with the dimensions mentioned in the electric field calculations. In the simulation, the microelectrode tip geometry was initially displaced $5 \mu\text{m}$ above the substrate and the calculated deposition profile updated using a maximum incremental deposition of $1 \mu\text{m}$ added to the points of maximum calculated surface velocity. Thus five cycles of calculation were necessary before any displacement of the microelectrode geometry was made. Consecutive tip displacements were $5 \mu\text{m}$ in the vertical direction above the substrate to form a column. Figure 10 shows the simulation results for the shape formation of a column up to $30 \mu\text{m}$ high.

To assess the validity of the results in figure 10, the obtained deposition profiles were compared against observed profiles of the deposition images in figure 6, which were

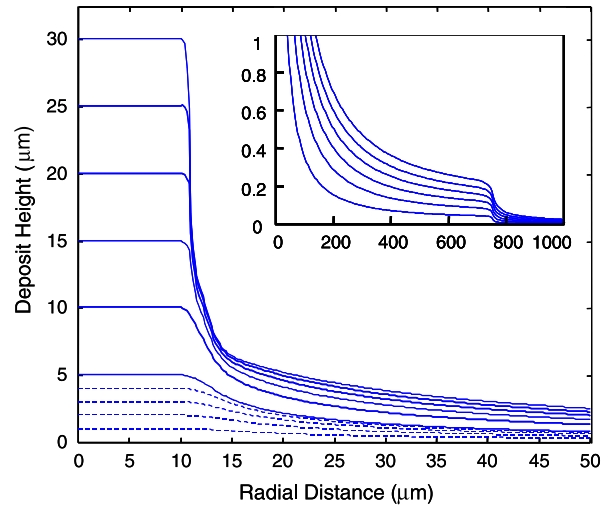


Figure 10. Deposition profiles of a column structure depositing over an infinite substrate, evaluated using the progressive boundary update approach. These profiles were calculated for a $5 \mu\text{m}$ progressive spacing between the microelectrode end and the deposition surface, with an incremental deposition of $1 \mu\text{m}$ as shown by the dashed curves.

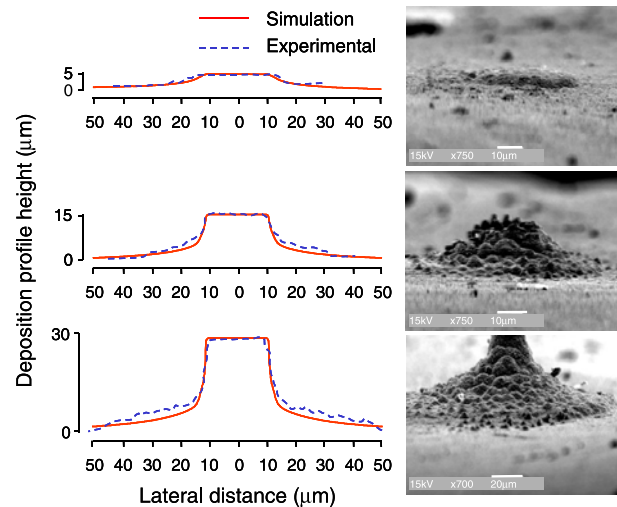


Figure 11. A comparison between deposition profiles of a column structure (diameter of $25 \mu\text{m}$) at different heights, obtained from the simulation results in figure 10 (solid curves), and the experimental results shown in figure 6 (dashed curves). Profiles from experimental results were obtained by processing the corresponding side-view images of figure 6, shown to the right, using contrast enhancement and edge detection.

extracted by processing side-view images of the same structures using contrast enhancement and edge detection. Figure 11 shows a comparison between the deposition profiles obtained from experimental deposition and from simulation using the proposed model, for the three deposition heights of 5, 15 and $20 \mu\text{m}$. The agreement between both profiles is very satisfactory.

The results in figure 10 provide a quantitative analysis as well as a reason for the enlarged side deposition at the column base. In general, the deposition profiles in figure 10 indicate that undesired deposition growth outside the region of the microelectrode tip (a circle with a radius of $12.5 \mu\text{m}$)

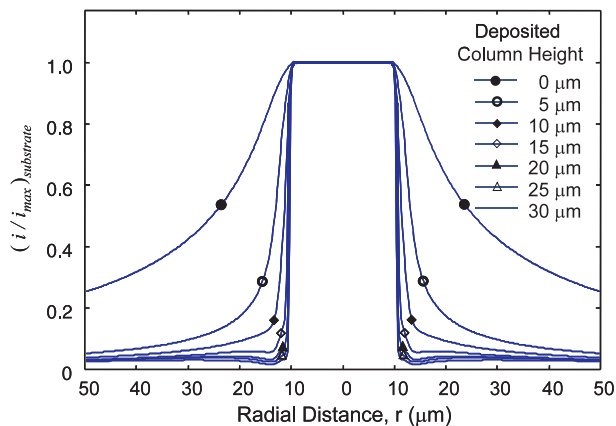


Figure 12. Calculated deposition current density profiles at the substrate and column surfaces for columns of the heights indicated in the figure. The calculated values are normalized relative to the deposition current density at $r = 0$.

is of a considerable rate relative to the rate of column growth, especially during the first 10–15 μm of the column's growth, thus producing the enlarged column base shown in figures 5 and 6. This is verified further in the calculations of the deposition current density profiles shown in figure 12. Here, the current density profiles at the substrate (beginning of column deposition, figure 9(b)) and at column surfaces (heights of 5, 10, 15, 20, 25 and 30 μm), are normalized relative to the current density at the centre of the column ($r = 0$). The calculated current density profiles in figure 12 suggest that deposition rates outside the region of the microelectrode tip reduce to negligible values (<5% of the rate at $r = 0$) when the microelectrode tip is almost one-half of a tip diameter away from the substrate. After separation of approximately one tip diameter between the microelectrode tip and the substrate, the deposition becomes very localized and contributes only to the formation of the column.

The reason for the increased deposition rate outside the tip region during the first 10–15 μm of column growth is explained by the insert in figure 10. Here, an enlarged view of the deposition profiles (by showing only the first 1 μm of the deposition) are shown up to a radial distance of 1000 μm (i.e. 250 μm beyond the extent of the glass insulation surrounding the electrode wire). First, the profiles shown suggest that when 30 μm of column height has been deposited the deposition at a radial distance as far as 300 μm would be about 0.5 μm . This would seriously limit the resolution of LECD. The results also show that the deposition drops abruptly around a radial distance of 750 μm , which is equivalent to the radius of the glass insulation surrounding the electrode wire. This leads to the conclusion that the glass surrounding the electrode wire enhances the side deposition, especially at small separations between the tip and the substrate. This is in agreement with the expected increase in the parasitic coupling between the electrode wire and the substrate due to the presence of the glass insulation, which has a dielectric constant higher than the electrolyte filling the space between the electrode and the substrate. Thus, an initial suggestion for reducing the undesired side deposition at the column base would be to reduce the extent of the glass insulation around the electrode wire. This is currently under investigation and will be utilized to enhance the resolution of LECD deposition.

5. Conclusion

Fabrication of high aspect ratio microstructures using LECD technology has been demonstrated. An experimental investigation and a theoretical model to quantitatively determine the shape formation of columnar like structures have been presented. Simulation procedures based on electric field calculation and the progressive boundary update method have been proposed to determine profiles of shape formation. Presented simulation results were compared against images of developing copper columns obtained experimentally at different stages of formation. Both results were in agreement and suggested that the glass insulation around the electrode wire can result in a reduced resolution of LECD. The results also demonstrate the importance of the proposed deposition model and simulation procedures as an analysis and design tool that can be used to further characterize and enhance fabrication by LECD technology.

Acknowledgments

The author would like to express his sincere appreciation to The Research Affairs at The United Arab Emirates University for the financial support of this project and the use of the technical facilities at the Central Laboratory Unit of the University. The author thanks Dr M I Hussein for providing the field calculation software.

References

- [1] Wolfenbuttel R F and Van Mullem C J 2001 *IEEE Trans. Instrum. Meas.* **50** 1469
- [2] Rebeiz G M, Katehi L P B, Ali-Ahmad W Y, Eleftheriades G V and Ling C C 1992 *IEEE Antennas Propag. Mag.* **34** 7
- [3] Herrick J, Yook J G and Katehi L P B 1998 *IEEE Trans. Microw. Theory Techn.* **46** 1832
- [4] Walker J A 2000 *J. Micromech. Microeng.* **10** R1
- [5] Gebhard M and benecke W 1995 *Proc. 1995 INRIA/IEEE Symp. on Emerging Technologies and Factory Automation 9*
- [6] Souteyrand E, Cloarec J P, Martin J R, Cabrera M, Bras M, Chauvet J P, Dugas V and Bessueille F 2000 *Appl. Surf. Sci.* **164** 246
- [7] Van Der Schoot B, Biollat M and De Rooij N 2001 *IEEE Trans. Instrum. Meas.* **50** 1538
- [8] Ikuta K, Hirowatari K and Ogata T 1994 *Proc. IEEE Micromech. Syst.* **1**
- [9] Robertson J K and Wise K D 1994 *Proc. IEEE Micromech. Syst.* **7**
- [10] El-Giar E M and Thomson D J 1997 *Proc. IEEE Conf. on Communications, Power and Computing WESCANEX 97* p 327
- [11] Dean R N Jr, Nordine P C and Christodoulou C G 2000 *Microw. Opt. Technol. Lett.* **24** 106
- [12] Rai-Choudhury P 1997 *Handbook of Microlithography Micromachining and Microfabrication* (Bellingham, CA: SPIE Optical Engineering Press) pp 1–2
- [13] Madiu M J 1997 *Fundamentals of Microfabrication* (Boca Raton, FL: Chemical Rubber Company Press)
- [14] Han J and Jensen K F 1994 *J. Appl. Phys.* **75** 2240
- [15] Brunger W H and Kohlmann K T 1992 *IEEE Microelectromech. Syst.* **92** 168
- [16] Hunter I W, Lafontaine S R and Madden J D 1997 *US Patent Specification* 5,641,391
- [17] Durney L J 1984 *Electroplating Engineering Handbook* 4th edn (New York: Van Nostrand-Reinhold)
- [18] Bard A J, Huesser O E and Craston D H 1990 *US Patent Specification* 4,968,390

- [19] Gelchinski M H, Romankiw L T, Vigliotti D R and Von Gutfeld R J 1985 *US Patent Specification* 4,497,692
- [20] Madden J D and Hunter I W 1996 *J. Microelectromech. Syst.* **5** 24
- [21] Yeo S H, Choo J H and Yip K S 2000 *Proc. SPIE* **4174** 30
- [22] Jasson A, Thornell G and Johansson S 2000 *J. Electrochem. Soc.* **147** 1810
- [23] Heb C, Borgwarth K, Ricken C, Ebling D G and Heinze J 1997 *Electrochim. Acta* **42** 3065
- [24] Lagraff J R and Gewirth A A 1994 *J. Phys. Chem.* **98** 12246
- [25] Müller A D, Müller F and Hietschold M 2000 *Thin Solid Films* **366** 32
- [26] El-Giar E M, Said R A, Bridges G E and Thomson D J 2000 *J. Electrochem. Soc.* **147** 586
- [27] Yeo S H and Choo J H 2001 *J. Micromech. Microeng.* **11** 435
- [28] Yeo S H, Choo J H and Sim K H A 2002 *J. Micromech. Microeng.* **12** 271
- [29] Said R A 2001 *The Electrochemical Society International Semiconductor Technology Conf. 2001 (Shanghai, China)*
- [30] Bard A J, Fan F-R F and Mirkin M V 1995 *Scanning Electrochemical Microscopy. Physical Electrochemistry: Principles, Methods, and Applications. I. Robenstein* (New York: Dekker) pp 209–42
- [31] Shigley J E 1977 *Mechanical Engineering Design* (New York: McGraw-Hill)
- [32] Bard A J and Mirkin M V 2001 *Scanning Electrochemical Microscopy* (New York: Wiley)
- [33] Alkire R, Bergh T and Sani R L 1978 *J. Electrochem. Soc.* **125** 1981
- [34] Sautebin R, Froidevaux H and Landolt D 1980 *J. Electrochem. Soc.* **127** 1096
- [35] Prentice G A and Tobias C W 1982 *J. Electrochem. Soc.* **129** 78
- [36] Sautebin R and Landolt D 1982 *J. Electrochem. Soc.* **129** 946
- [37] Hume E C, Deen W M and Brown R A 1984 *J. Electrochem. Soc.* **131** 1251
- [38] Deconinck J, Maggetto G and Vereecken J 1985 *J. Electrochem. Soc.* **132** 2960
- [39] Paunovic M and Schlesinger M 1998 *Fundamentals of Electrochemical Deposition* (New York: Wiley)
- [40] Bard A J and Faulkner R 1980 *Electrochemical Methods: Fundamentals and Applications* (New York: Wiley)
- [41] Greef R, Peat R, Peter L M, Pletcher D and Robinson J 1985 *Instrumental Methods in Electrochemistry* (New York: Halsted Pr)
- [42] Prentice G A and Tobias C W 1982 *J. Electrochem. Soc.* **129** 72
- [43] Brebbia C A 1984 *The Boundary Element Method for Engineers* (London: Pentech)